Stochastic Finite-Fault Simulation of 22 February 2005 (Mw 6.4) Zarand Earthquake (Iran), based on Dynamic Corner Frequency

Behzad Hassani
School of Civil Engineering, University of Tehran, Email: behhassani@gmail.com

Hamid Zafarani
Assistant Professor, International Institute of Earthquake Engineering and Seismology *(IIEES)*

Jamshid Farjoodi
Assistant Professor, School of Civil Engineering, University of Tehran

SUMMARY:
Horizontal components of 14 Strong-motion accelerograms were exploited to obtain simulation parameters of 22 February 2005, moment magnitude M 6.4 Zarand (central Iran) earthquake. The stochastic finite-fault modeling based on dynamic corner frequency was implemented to simulate the event. To perform the simulation, the site responses and the attenuation parameters were selected from regional seismic studies. Furthermore, the two free source parameters, namely stress drop ($\Delta\sigma$) and pulsing area percentage are achieved by minimizing the model error of the acceleration response spectra in the frequency band of 0.4-15 Hz. We found that the $\Delta\sigma$=32 and the pulsing area percentage equals to 50% provide the best fit to the observed response spectra and peak ground acceleration (PGA).

Keywords: Stochastic finite-fault modeling; dynamic corner frequency; simulation of Zarand earthquake

1. INTRODUCTION

Iranian plateau, located along the Alpine-Himalayan orogenic belt, is one of the most highly seismic regions of the world. Many devastating earthquakes have occurred during the long history of this ancient country (Fig. 1.1). Continental coverage of about 35 mm/yr between the Eurasian and Arabian plates is absorbed in Iran by strike-slip and reverse faults (Jackson et al., 1995). However the active deformation is not uniformly distributed and no single fault accommodates a large percentage of plate convergence (Berberian & Yeats, 1999). The most active seismic zones, in decreasing order of activity, are: Zagros, Alborz and East-Central Iran (Berberian, 1976; Takin, 1972). Central Iran is characterized by scattered seismic activity with large magnitude earthquakes, long recurrence periods and seismic gaps along several Quaternary faults. The earthquakes in the zone are generally shallow and are usually associated with surface faulting (Berberian, 1976; 1979). On 22 February 2005 at 02:25 GMT, a shallow destructive earthquake of Mw 6.4 occurred in east of Zarand town (central Iran), about 60 km north of the city of Kerman, the provincial capital. The earthquake demolished much of the town and other nearby villages. Number of victims reached more than 600 people. Many of the structures in the region were poorly designed mud-constructions that collapsed quickly on sleeping inhabitants. The focal mechanism solutions as well as field observation show that this earthquake involved thrust faulting on a plane striking nearly east-west and dipping towards the north (Talebian et al., 2006). Twenty seven strong-motion instruments (SSA-2 accelerometers) of the Building and Housing Research Center of Iran (BHRC), located mainly within the state of Kerman, recorded the mainshock. According to Talebian et al. (2006), the 2005 Zarand earthquake involved reverse faulting, unlike the strike-slip faulting responsible for the earlier recent earthquakes in this zone, and it had a northward dip of about 67°, which is steep even for reverse faults. In this article, we use strong-motion records from 14 stations azimuthally well distributed to find the necessary source and propagation parameters for the stochastic model proposed by Motazedian and Atkinson (2005).

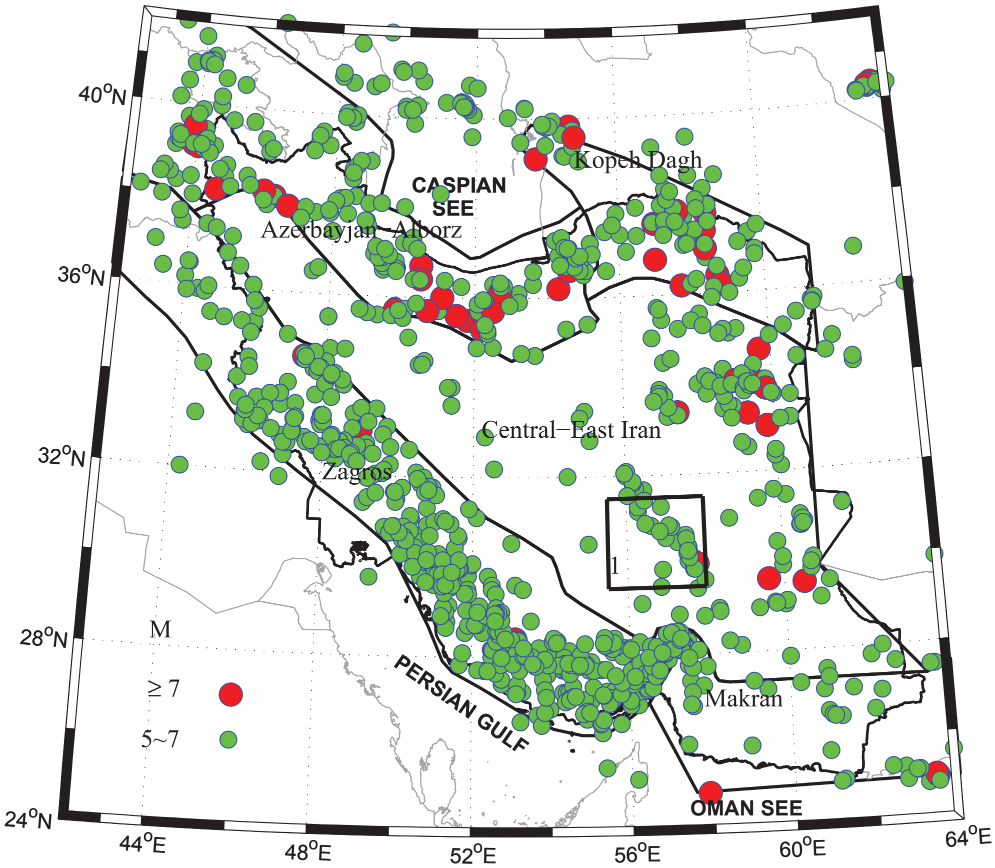

Figure 1.1. Earthquakes in Iranian plateau from 3000 BC up to 2005 (Berberian & Yeats, 1999), and Principal seismotectonic zones of Iran according to Mirzaei et al. (1998). The region which covers Zarand event is also shown as region 1.

2. DATA

Fig. 2.1. shows the distribution of the 14 stations selected for the analyses and the location of the earthquake epicenter beside the surface projection of the fault. Furthermore, it depicts the rupture area (rectangle) and epicentral location of the event. All of the available records were taken from BHRC Database. We selected records from stations located on free-field sites with clear P- and S-wave arrivals which are correctable using Multi-resolution wavelet analysis (Ansari et al., 2007; 2010). Table. 2.1. lists the coordinates and site characteristics of these stations.. The recording instruments are digital accelerographs (Kinemetrics SSA-2), installed at distances ranging from 17 to 104 km with respect to the epicenter of the examined earthquake. The maximum peak ground acceleration is as much as 481 cm/s/s and was recorded at the Shirinrood Dam1 station. Detailed information on the locations and the geological conditions at the installation sites, as well as PGA values recorded during the examined earthquake is given in Table. 2.1. Moreover, the PGA of the synthetic accelerations is presented in this table which the procedure to simulate the accelerations is described in the following section.

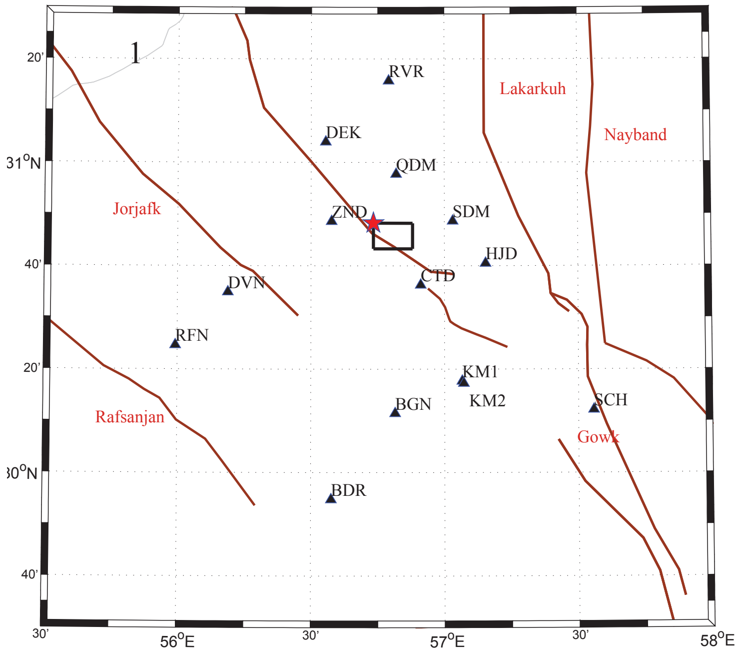

Figure 2.1. Epicentral location of Zarand earthquake and distribution of stations used in this study. The rupture intiation point (star) and the surface projection of the fault (rectangle) are also shown.

Table 2.1. Recording characteristics of the strong-motion stations

Code	Station Name	Latitude	longnitude	Hypocentral distance (km)	site Class	PGA/L (cm/s/s)	PGA/T (cm/s/s)	PGA/(Synth) (cm/s/s)
SCH	Sirch	30.20	57.56	104	Rock	13	8	14
RVR	Ravar	31.26	56.79	51	Soil	120	74	119
KM1	kerman1	30.30	57.07	66	Soil	33	30	36
BGN	Baghin	30.19	56.82	69	Soil	27	23	29
BDR	Bardsir	29.91	56.58	101	Rock	10	13	13
ZND	Zarand	30.81	56.58	17	soil	312	234	239
CTD	Chatrood	30.61	56.91	29	Rock	54	94	64
SDM	Shirinrood Daml	30.81	57.03	29	Rock	481	200	288
DEK	Dasht-e-Khak	31.07	56.56	34	Soil	49	61	67
KM2	Kerman 2	30.29	57.07	67	Soil	24	26	24
HJD	Horjand	30.68	57.15	43	Soil	47	42	51
QDM	Qadrooni Dam	30.96	56.82	20	Rock	212	137	202
DVN	Davaran	30.58	56.19	59	Rock	54	47	26
RFN	Rafsanjan	30.41	55.99	84	Soil	23	20	31

3. SIMULATION METHOD AND PARAMETERS

The procedure which is used for the generation of high frequency components of ground motion is the widely applied stochastic finite-fault method (Beresnev and Atkinson, 1997) which was modified by Motazedian and Atkinson (2005). In former finite-fault method by changing the number of subfaults, the total radiated energy from the entire fault is not conserved (Motazedian & Atkinson,2005, Figure 1). The later authors introduced the concept of dynamic corner frequency to overcome the common disadvantages of the finite-fault method. In this promoted model, the corner frequency is a function of time, and the rupture history controls the frequency content of the simulated time series of each subfault. The rupture begins with a high corner frequency and progresses to lower corner frequencies as the ruptured area grows. Limiting the number of active subfaults in the calculation of dynamic corner frequency can control the amplitude of lower frequencies. The dynamic corner frequency approach has several advantages over previous formulations of the stochastic finite-fault method, including conservation of radiated energy at high frequencies regardless of subfault size, application to a broader magnitude range, and control of the relative amplitude of higher versus lower frequencies. In this method the ground motion acceleration, $a(t)$, from the entire fault is given by

$$a(t) = \sum_{i=1}^{nl} \sum_{j=1}^{nw} a_{ij}(t + \Delta t_{ij}) \tag{3.1}$$

where *nl* and *nw* are the number of subfaults along the length and width of main fault, respectively and Δt_{ij} is the relative delay time for the radiated wave from the *ij*th subfault to reach the observation point. The $a_{ij}(t)$ are each calculated by the stochastic point-source method as described by Boore (1983). The acceleration spectrum for a subfault at a distance R_{ij} is modeled as a point source with an ω^2 shape (Aki, 1967; Brune, 1970; Boore 1983). The acceleration spectrum of shear wave of the *ij*th subfault, $A_{ij}(f)$, is described as follows

$$\begin{aligned} A_{ij}(f) = \{C\, M_{0ij} H_{ij} (2\pi f)^2 / [1 + (f / f_{0ij}(t))^2]\} \\ \{\exp(-\pi f R_{ij} / Q(f)\beta_s) \exp(-\pi \kappa_0 f) Z(R_{ij})\}\{G(f)\} \end{aligned} \tag{3.2}$$

where M_{0ij}, and R_{ij} are the *ij*th subfault seismic moment, corner frequency, and distance from the observation point, respectively. The constant $C=(R_{\Theta\Phi})VF/(4\pi\rho_s\beta_s^3R_0)$, where $R_{\Theta\Phi}$ =0.55 is the average shear-wave radiation pattern, F=2 is the free surface amplification, $V = 1/\sqrt{2}$ is introduced to account for dividing the total shear-wave energy into two horizontal components, ρ_s=2.8 gr/cm3 and β_s=3.5 km/s are the mass density and the shear-wave velocity in the vicinity of the earthquake source, respectively and R_0=1 km is a reference distance. H_{ij} is a scaling factor that is applied to conserve the high-frequency spectral level of subfaults and $f_{0ij}(t)$ is the dynamic corner frequency which can be defined as a function of $N_R(t)$, the cumulative number of ruptured subfaults at time t (Motazedian & Atkinson, 2005),

$$f_{0ij}(t) = N_R(t)^{-1/3} \times 4.9 \times 10^6 \times \beta_s (\Delta\sigma / M_{0ave})^{1/3} \tag{3.3}$$

where M_{0ave} is the average seismic moment of subfaults and $\Delta\sigma$ is the stress drop in bars. The diminution parameter or zero-distance kappa factor κ_0, the quality factor $Q(f)$ and the geometrical spreading are assumed as 0.05,151 $f^{0.75}$ and, R_{ij}^{-1} for R_{ij}< 60 km and $(R_{ij}.60)^{-0.5}$ for $R_{ij} \geq$ 60 km, respectively, which are presented for Central-East region by Hassani et al.(2011). They used generalized inversion method to estimate the earthquake parameters namely source, path and site effects. Moreover, using their study, we have access to a proper estimation of site amplification $G(f)$ to substitute in Eqn. 3.2. and simulate the time series more accurately.

According to Eqn. 3.3., as the rupture propagates toward the end of the fault, the number of ruptured subfaults increases; hence, the corner frequency of the subfaults decreases. It means that the dynamic corner frequency tends to decrease the level of the spectrum of the subfaults and consequently their radiated energy at high frequencies. To deal with this issue, a scaling factor was introduced to conserve the high-frequency spectral level and accordingly the total level of radiated energy. The scaling factor, H_{ij}, implies that the radiate energy of the whole fault should be N times greater than the radiated energy from *ij*th subfault (Motazedian and Atkinson, 2005).

Pulsing subfults is another concepts that is introduced in this method. In actual earthquake ruptures, the slip may only be occurring on part of the fault at any one time. Heaton (1990) proposed the concept of a "self-healing" model, in which the duration of slip at any location on the fault is short. Using pulsing subfaults concept, we can consider a form of this behavior, in which just only part of the fault is actively pulsing at any time. For example, a pulsing area of 25% means that during the rupture of a subfault, at most, 25% of all the subfaults are active and the remaining subfaults are passive. According to this concept, the cumulative number of pulsing subfaults, as given by $N_R(t)$ in Eqn. 3.3., increases with time at the beginning of rupture but becomes constant after a while, at some fixed percentage of the total rupture area. Thus, the dynamic corner frequency decreases with time near the beginning of the rupture and then becomes constant.

Variation of pulsing subfaults can be used to adjust the relative amplitudes of low-frequency motion in finite-fault modeling. On the other hand, the stress drop (Eqn. 3.3) is a parameter which is used to adjust the high-frequency spectral amplitudes and high-frequency energy. Therefore, these are the two main free parameters of the model.

To calibrate the input parameters of the model, the bias was defined as:

$$E(f) = \frac{1}{n}\sum_{i=1}^{n} \log\left(\frac{PSA(f)_{obs}}{PSA(f)_{sim}}\right)_i \tag{3.4}$$

and the average error as

$$\varepsilon = \frac{1}{m}\sum_{i=1}^{m} E_j(f) \tag{3.5}$$

where n is the number of stations, $PSA(f)_{obs}$ is horizontal component of 5% damped pseudoacceleration spectrum, and m is the number of frequencies used to calculate the average. The simulated $PSA(f)_{sim}$ was obtained using the finite-fault radiation simulation code EXSIM (Motazedian and Atkinson, 2005). This code uses the Boore (1983) procedure to simulate a time series using an acceleration spectrum of a subfault (Eqn. 3.2) and exploits it to produce the time series corresponding to the total fault plane (Eqn.3.1). All the parameters which are used for the simulation in EXSIM, are summarized in Table. 3.1.

Table 3.1. Modeling parameters used for the simulation method

Parameter	Parameter Value
Fault orientation (strike/dip) (Degree)	270 / 67
Fault dimensions along strike and dip (km)	14, 10
Location of rupture initiation point	30.804° N, 56.734° E (BHRC)
Depth to the top of the Fault (km)	0.0
Mainshock moment magnitude (Mw)	6.4
Crustal shear-wave velocity (km/s)	3.5
Rupture velocity (km/s)	0.8× shear-wave velocity
Crustal density (g/cm3)	2.8
$Q(f)$	$Q(f)=151f^{0.75}$
Windowing function	Saragoni-Hart
Geometric spreading	R^{-1} ($R\leq 60$ km), $(R.60)^{-1/2}$ ($R > 60$ km)
Site amplification	Generalized Inversion Method (Hassani et al., 2011)
Kappa (parameter of high-cut filter, sec)	0.05

4. RESULTS

To calibrate the model parameters, we performed the simulations for a wide range of values of stress drop and pulsing area percentage to allow a grid search of the model error (ε). The lowest residuals averaged over all events and all frequencies from 0.4 Hz to 15 Hz are obtained for a stress drop of 32 bars with a

50% pulsing area, which also results in the estimation of PGA for simulated time series (Table. 1.1). Fig. 4.1. shows the bias ($E(f)$) versus frequency for the case of 32 bars stress drop and 50% pulsing area. The model bias is close to zero at all frequencies with a small standard deviation. Moreover, In Fig. 4.2 for some stations, the results of the stochastic simulations and their comparisons with the observed strong ground-motion records are presented. In general, the synthetics are in good agreement with observations in almost all cases.

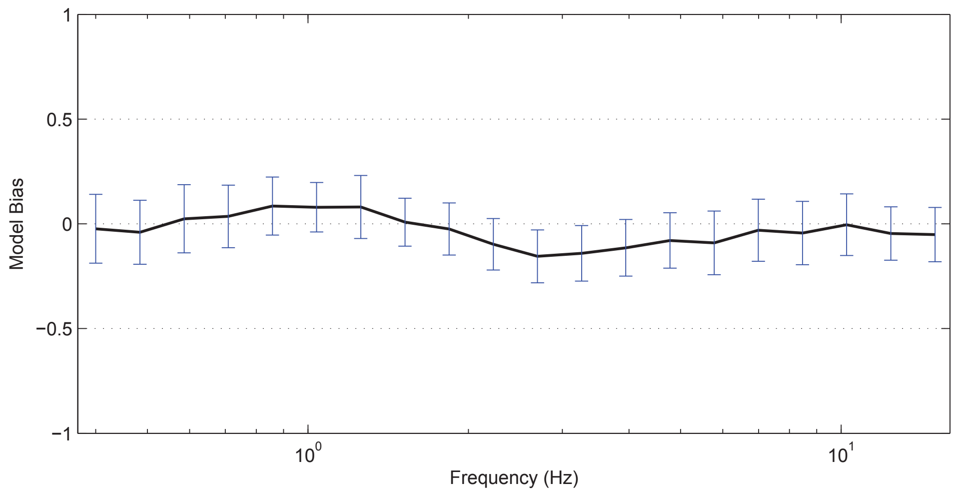

Figure 4.1. The bias calculated for the case of 32 bars stress drop and 50% pulsing area.

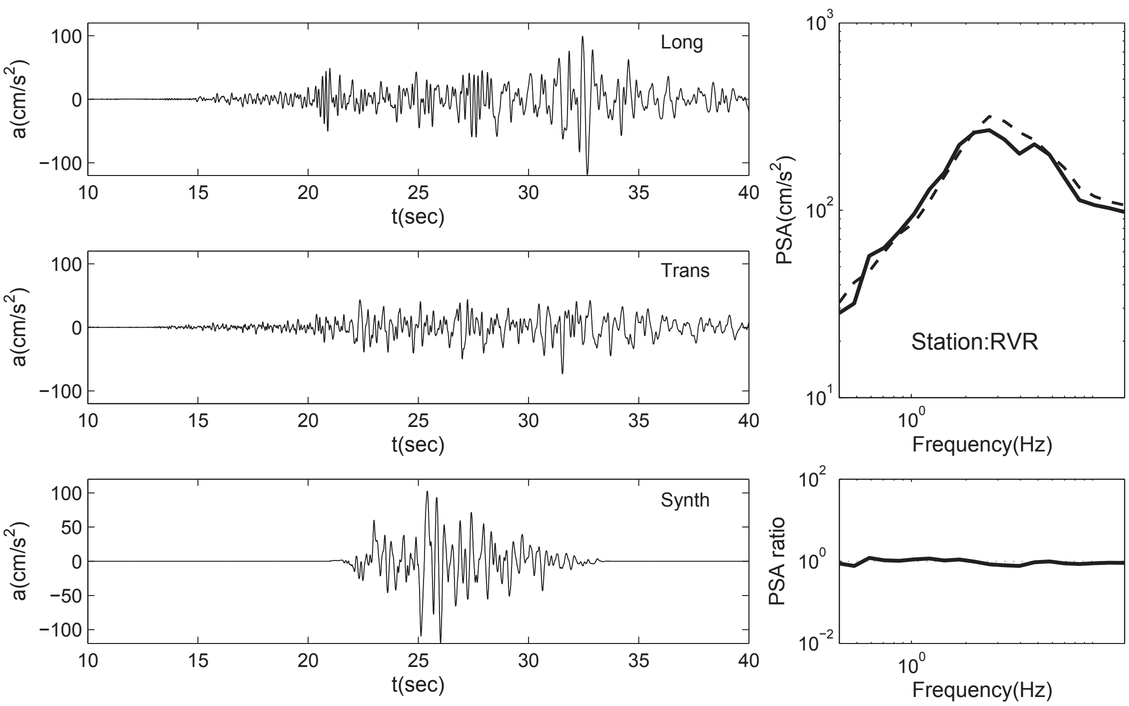

Figure 4.2. Comparison of the simulated acceleration time series with observed records (left). The $PSA(f)_{obs}$ (solid) and $PSA(f)_{sim}$ (dashed) are also shown (right-top). The ratio of observed to simulated spectra is also shown (right-down). (Figure continues on following pages)

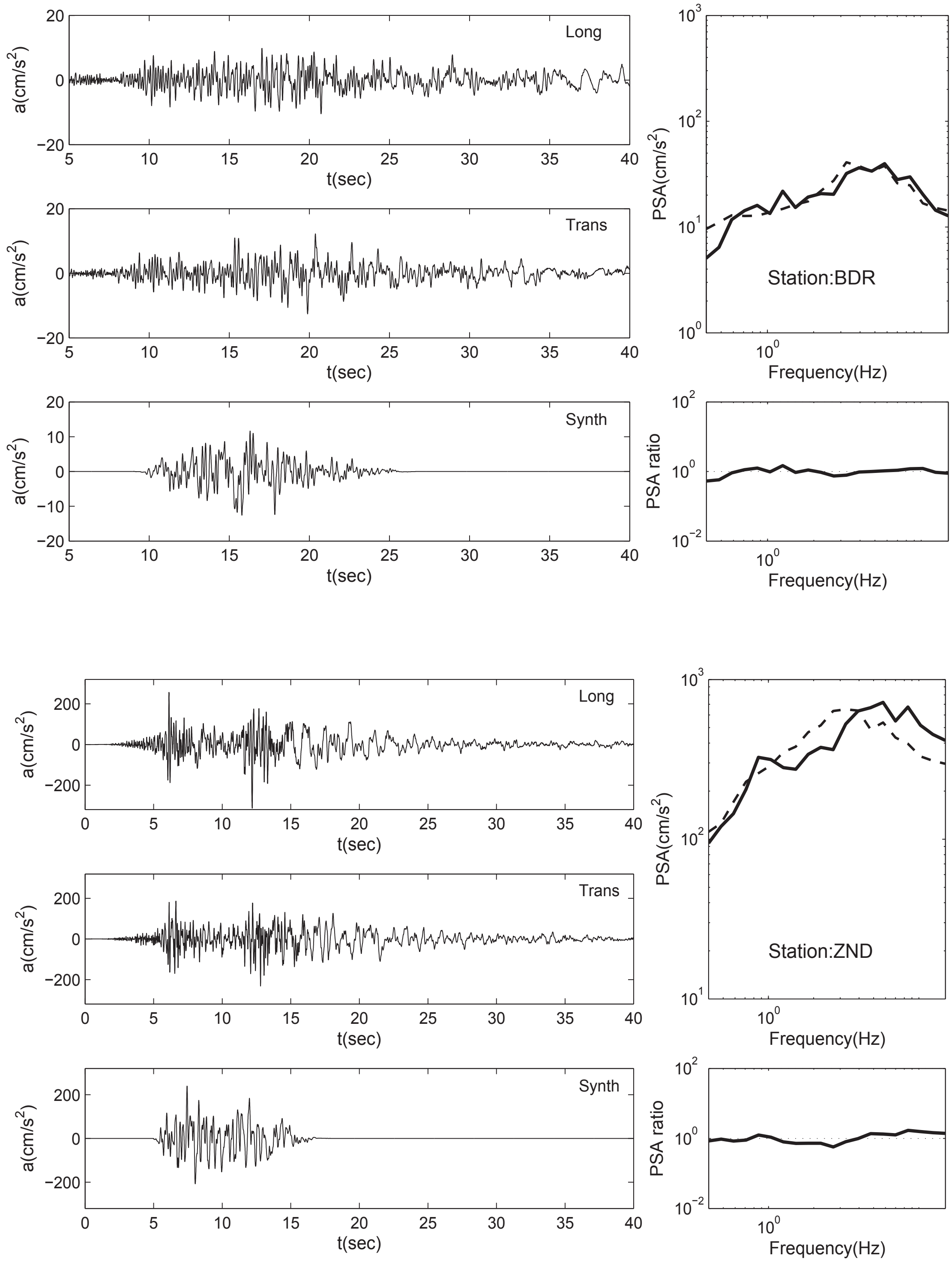

Figure 4.2. Continued

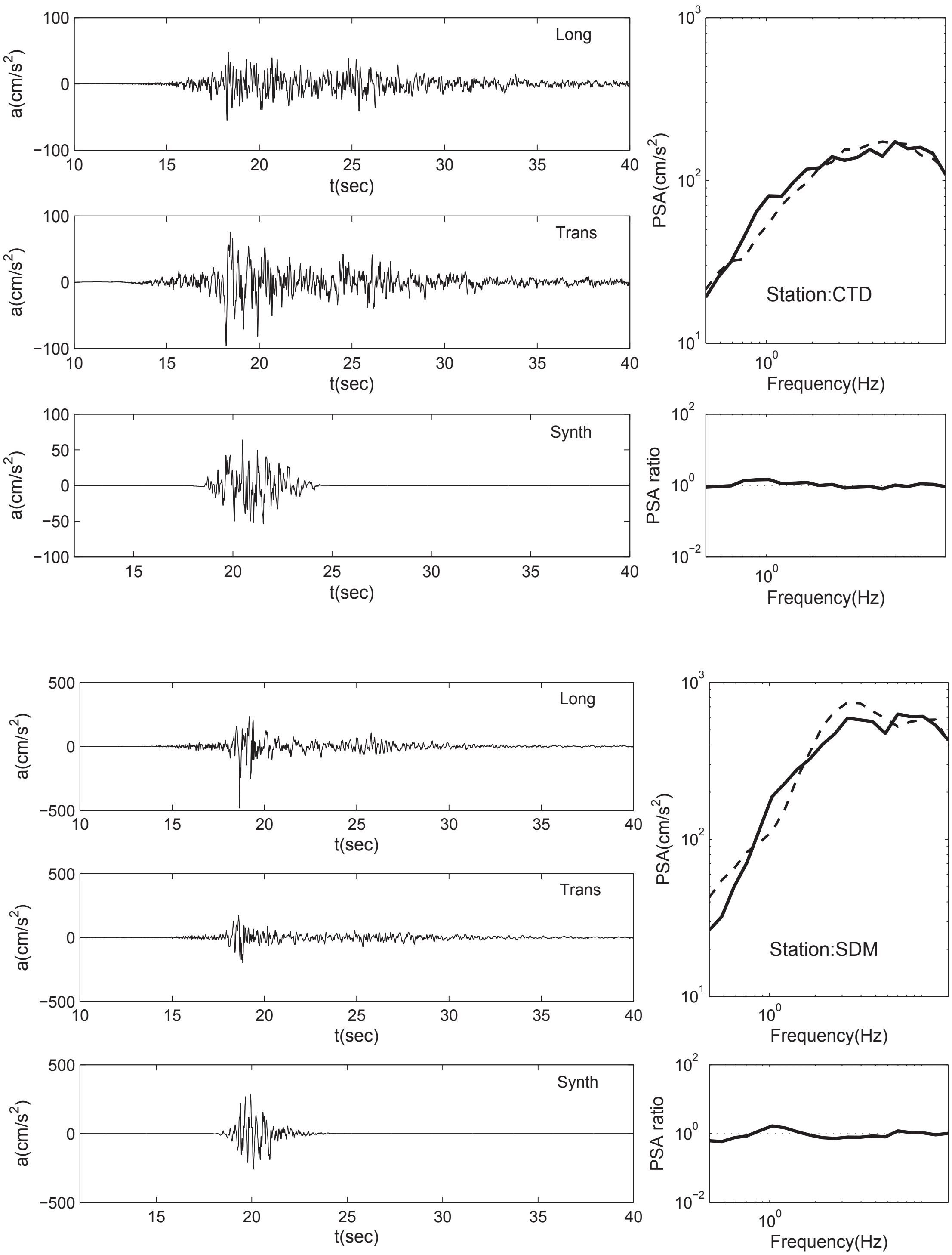

Figure 4.2. Continued

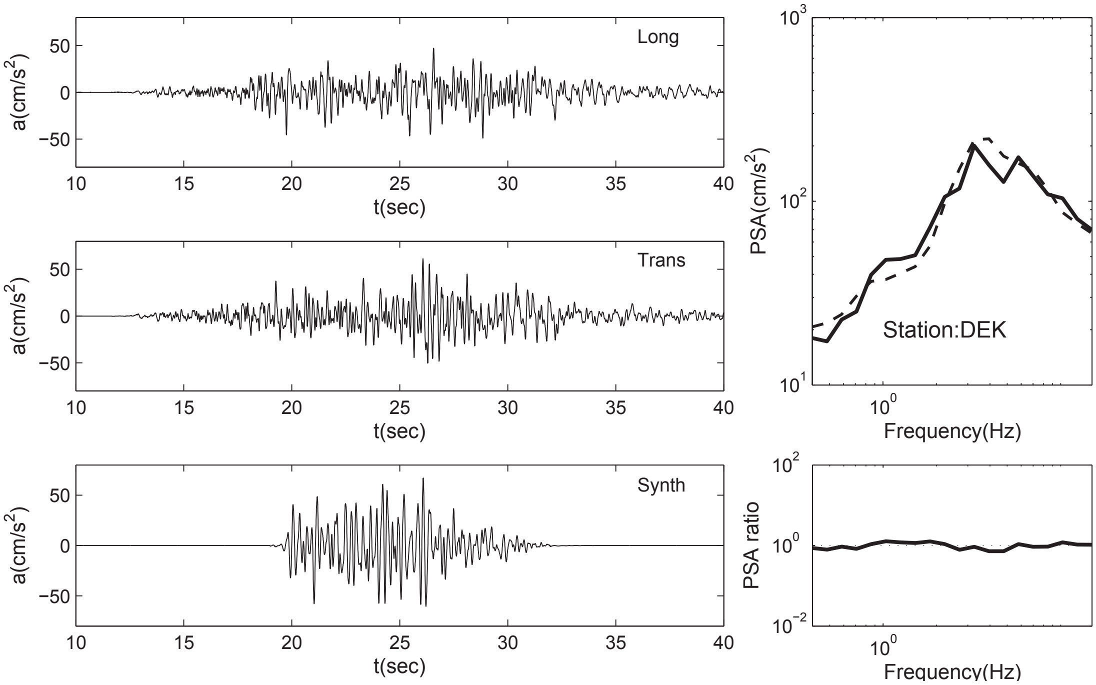

Figure 4.2. Continued

5. CONCLUSION

Using available information about the fault rapture of Zarand earthquake, besides employing appropriate assumption about attenuation parameters and site amplification from regional studies, the simulation parameters were obtained for this event in 0.4-15 Hz frequency band. The model error (ε) was optimized by varying two free model parameters, namely pulsing area percentage and stress drop. The model bias $E(f)$ is close to zero at all frequencies, and also the PGA of the simulated time series are completely consistent with observed ones.

One the main advantages of this study over similar investigations is using regional earthquake parameters instead of some simplified assumptions. Previously Zafarani et al. (2007) used the stochastic finite-fault modeling with static corner frequency to obtain the simulation parameters for this event. Facing deficiency of enough information about regional attenuation parameters and site amplifications, they used some simple assumptions to resolve this issue. Moreover, as mentioned before, static corner frequency has some disadvantages comparing with the approach which is used in this study.

AKNOWLEDGMENT

The authors acknowledge the Building and Housing Research Center of Iran for providing them with the accelerograms used in the current study.

REFERENCES

Aki, K. (1967). Scaling law of seismic spectrum. *Journal of Geophysical Research* **72**, 1217–1231.

Ansari, A., Noorzad, A. and Zare, M. (2007). Application of wavelet multi-resolution analysis for correction of seismic acceleration records. *Journal of Geophysics and Engineering* **4**, 1–16.

Ansari, A., Noorzad, A., Zafarani, H. and Vahidifard, H. (2010). Correction of highly noisy strong motion records using modified wavelet de-noising method. *Soil Dynamic and Earthquake Engineering* **30**, 1168–81.

Berberian, M. (1976). Contribution to the seismotectonics of Iran (Part II), Geological Survey of Iran, Rep. No.39.

Berberian, M. (1979). Earthquake faulting and bedding thrust associated with the Tabas-E-Golshan (Iran) earthquake of September 16, 1978. *Bulletin of the Seismological Society of America* **69**, 1861-1887.
Berberian, M. and Yeats, R.S. (1999). Patterns of historical earthquake rupture in the Iranian plateau. *Bulletin of the Seismological Society of America* **89**, 120-139.
Beresnev, I.A. and Atkinson, G.M. (1997). Modeling finite-fault radiation from the Omega-n spectrum. *Bulletin of the Seismological Society of America* **87**, 67-84.
Boore, D. (1983). Stochastic simulation of high-frequency ground motions based on seismological models of the radiated spectra. *Bulletin of the Seismological Society of America* **73**, 1865–1894.
Brune, J. (1970). Tectonic stress and the spectra of seismic shear waves from earthquakes. *Journal of Geophysical Research* **75**, 4997–5009.
Hassani, B., Zafarani, H., Farjoodi, J. and Ansari, A. (2011). Estimation of Site Amplification, Attenuation and Source Spectra of S-Waves in the East-Central Iran. *Soil Dynamic and Earthquake Engineering* **31**, 1397-1413.
Heaton, T. (1990). Evidence for and implications of self-healing pulses of slip in earthquake rupture. *Physics of the Earth and Planetary Interiors* **64**, 1–20.
Jackson, J.A., Haines, J. and Holt, W. (1995). The Accommodation of Arabia-Eurasia Plate Convergence in Iran. *Journal of Geophysical Research* **100**, 15205–15219.
Mirzaei, N., Mengtan, G. and Yuntai, C. (1998). Seismic source regionalization for seismic zoning of Iran: Major seismo tectonic provinces. *Earthquake Prediction Research* **7**, 465–95.
Motazedian, D. and Atkinson, G. M. (2005). Stochastic finite-fault modeling based on a dynamic corner frequency. *Bulletin of the Seismological Society of America* **95**, 995–1010.
Takin, M. (1972). Iranian geology and continental drift in the Middle East. Nature 235 No.5334, 147-150.
Talebian, M. Biggs, J., Bolourchi, M., Copley, A., Ghassemi, A., Ghorashi, M., Hollingsworth, J., Jackson, J., Nissen, E., Oveisi, B., Parsons, B., Priestley, K. and Saiidi, A. (2006). The Dahuiyeh (Zarand) earthquake of 2005 February 22 in central Iran: reactivation of an intramountain reverse fault. *Geophysical Journal International* **164**, 137–148.
Zafarani, H., Noorzad, A. and Bargi, K. (2007). Stochastic Finite-Fault Strong Ground-Motion Simulation of The 22 February 2005 (Mw 6.4) Zarand (Central Iran) Earthquake. *4th International Conference on Earthquake Geotechnical Engineering*. Paper No.1147.